Accepted Manuscript

Late Holocene sea-level evolution of Paros Island (Cyclades, Greece)

Anna Karkani, Niki Evelpidou, Matthieu Giaime, Nick Marriner, Christophe Morhange, Giorgio Spada

PII: S1040-6182(18)31240-0

DOI: https://doi.org/10.1016/j.quaint.2019.02.027

Reference: JQI 7768

To appear in: *Quaternary International*

Received Date: 26 November 2018

Revised Date: 14 February 2019

Accepted Date: 18 February 2019

Please cite this article as: Karkani, A., Evelpidou, N., Giaime, M., Marriner, N., Morhange, C., Spada, G., Late Holocene sea-level evolution of Paros Island (Cyclades, Greece), *Quaternary International* (2019), doi: https://doi.org/10.1016/j.quaint.2019.02.027.

Late Holocene sea-level evolution of Paros Island (Cyclades, Greece)

Karkani Anna[1*], Evelpidou Niki[2], Giaime Matthieu[3], Marriner Nick[4], Morhange Christophe[5], Spada Giorgio[6]

[1] Faculty of Geology and Geoenvironment, National and Kapodistrian University of Athens, Panepistimiopolis, Zografou, 15784 Athens, Greece, email: ekarkani@geol.uoa.gr

[2] Faculty of Geology and Geoenvironment, National and Kapodistrian University of Athens, Panepistimiopolis, Zografou, 15784 Athens, Greece, email: evelpidou@geol.uoa.gr

[3] University of Durham, Department of Geography, South Road, DH1 3LE, Durham, UK, email: matthieu.giaime@gmail.com

[4] CNRS, Laboratoire Chrono-Environnement UMR6249, Université de Franche-Comté, UFR ST, 16 Route de Gray, 25030 Besançon, France, email: nick.marriner@univ-fcomte.fr

[5] Aix Marseille University, CNRS, IRD, Coll France, CEREGE, Aix-en-Provence, France; RIMS, The Leon Recanati Institute for Maritime Studies University of Haifa, 31905, Israel , email: morhange@cerege.fr

[6] Dipartimento di Scienze Pure e Applicate (DiSPeA), Università di Urbino “Carlo Bo”, Italy, email: giorgio.spada@gmail.com

* corresponding author

Abstract

Relative sea-level (RSL) reconstructions are essential to answer a variety of scientific questions, ranging from the investigation of crustal movements to the calibration of earth rheology models and ice sheet reconstructions.

It is generally assumed that most Cycladic islands (Aegean Sea, Greece) are affected by a gradual subsidence, attributed to the crustal thinning and to hydro-isostatic processes that accompanied the post-glacial rise in sea level. In this paper, we produce new RSL data from sedimentary records on Paros Island. We compare and contrast these RSL data with published data from the nearby island of Naxos. Our results are further compared with sea-level predictions from two different GIA models in an attempt to better quantify the tectonic regime of the wider study area. Our findings suggest average tectonic subsidence rates close to 1.0±0.4 mm/yr since 5500 cal BP. These rates are not linear in time and have increased since 2500 cal BP.

Keywords: relative sea level, subsidence, coastal geomorphology, lagoon, Holocene, central Aegean

1. Introduction

Sea-level changes are driven either by variations in the masses or volume of the oceans, defined as ‘eustatic’, or by changes of the land with respect to the sea surface, called ‘relative’ (Rovere *et al.*, 2016). During the past 4000 years, the ice-equivalent melt-water input is considered minimal (Peltier, 2002; Milne *et al.*, 2005; Church *et al.*, 2008). Therefore, any significant changes in relative sea-level (RSL) are almost entirely driven by vertical land movements caused by tectonics and glacial isostatic adjustment (GIA) or sediment compaction (Engelhart *et al.*, 2009).

RSL reconstructions are key to probing various research questions, ranging from the calibration of earth rheology models and ice sheet reconstructions to the investigation of crustal movements (Lambeck *et al.*, 2004; Peltier, 2004; Engelhart and Horton, 2012). GIA models have often been employed to identify stable and unstable areas and deduce tectonic rates through comparisons with observational data (e.g. Sivan *et al.*, 2001; 2004; Pirazzoli, 2005; Pavlopoulos *et al.*, 2011; Stiros et al., 2011; Van De Plassche et al., 2014; Woodroffe et al., 2015; Bradley et al., 2016; Chelli *et al.*, 2017; Vacchi *et al.*, 2017; Melis *et al.*, 2018). Greece, like the rest of the Mediterranean, is characterized by small tidal ranges that favor the preservation of sea level indicators (e.g. Rovere *et al.*, 2012).

In this context, the main aim of this study is to elucidate the relative sea-level history of Paros island during the Late Holocene (i.e., last 4000 years), through the multiproxy analysis of a sediment core from the western part of the island, in combination with published data from the central Cyclades. We compare and contrast our results with new modelled curves for Paros island, in an attempt to reconstruct RSL changes and assess the tectonic regime of the central Cyclades.

2. Regional Setting

The Cycladic Plateau has been subjected to successive stages of emergence and submergence due to changing sea level during the Quaternary (Kapsimalis *et al.*, 2009). The central Aegean is considered to be an area of low seismicity, characterized by the absence of large earthquakes (Fig. 1) (e.g. Papazachos, 1990; Sakellariou and Galanidou, 2016). According to Sakellariou and Galanidou (2016), vertical tectonic movements are of minor significance and the coastal evolution of the central Aegean

during Late Pleistocene-Holocene is mostly affected by eustatic sea-level fluctuations and, to a lesser degree, by isostatic movements.

Lykousis (2009) noted a continuous subsidence rate during the last 400 ka, with values of 0.34–0.60 mm/yr for the Cycladic plateau, with a gradual decrease in the magnitude of the extensional tectonic regime. According to Tirel *et al.* (2004), the Cyclades probably act as a rigid block translated toward the south–west with no significant deformation, in agreement with GPS velocities and a lack of major earthquakes.

The Island of Paros lies in the central Aegean Sea, constituting the third largest island in the Cyclades archipelago (Fig. 1, 2). Paros forms a NE–SW trending dome bounded by a low-angle inactive normal fault to the east and northeast (Bargnesi *et al.*, 2013). It has a rocky coastal zone, particularly in the northern part, characterized by the alternation of carbonate rocks, gneisses-schists and alluvial deposits (Papanikolaou, 1996). Beaches form a smaller part of coastal zone, mainly near coastal plains in the eastern part of the island.

The coring site, Pounta (POU2) is located in the western coast of Paros (Fig. 2a). POU2 core was drilled on the southwest coast, 1 km south of Pounta (Fig. 2a, b). Today, the area is characterized by the presence of coastal dunes, forming a sandy spit/barrier that frames a leeward lagoon.

3. Materials and Methods

3.1 Palaeoenvironmental reconstruction

A borehole was drilled with a portable drilling sampler, 35 mm in diameter, reaching a maximum depth of 4 m below mean sea level (msl). For the palaeoenvironmental reconstruction, multiproxy analyses were undertaken, which included

sedimentological analysis of the core, biostratigraphy of the macrofauna and ostracods and radiocarbon dating.

The core was analyzed at Chrono-environment (CNRS, University of Franche-Comté, Besançon, France). The core was first studied and photographed in detail in order to record the general stratigraphy. The sediment texture was determined by separating out the gravel (>2 mm), sand (2 mm to 50 μm) and silt/clay (<50 μm) fractions, using two sieve mesh sizes, 2 mm and 50 μm.

The gravel fraction of the sediments was examined to identify mollusc shells and determine their ecology. The identifications and classifications are based on d' Angelo and Gargiullo (1978) and Doneddu and Trainito (2005). The species were assigned to ecological groups defined by Pérès and Picard (1964) and Pérès (1982). Ostracods were extracted from the dry sand fraction (>150 μm). The identified taxa were assigned to assemblages based on their ecological preferences: freshwater, lagoonal, marine lagoonal, coastal and marine (Lachenal, 1989; Nachite *et al.*, 2010; Salel *et al.*, 2016).

3.2 Chronology

The chronostratigraphy of the core is based on four AMS radiocarbon dates performed at the Poznan Radiocarbon Laboratory (Poland) (Table 1). The radiocarbon ages of the samples were calibrated using the online software Calib 7.10 (Stuiver *et al.*, 2016) with the Marine13 curve (Reimer *et al.*, 2013). Ages of the shell samples were corrected for the local marine reservoir effect according to Reimer & McCormac (2002), using a mean ΔR value of 154 ± 52 for the Aegean Sea.

3.3 Sea-level reconstruction

Results of the paleo-environmental reconstruction of the new core revealed facies characteristic of coastal and lagoonal environments. We produced a new suite of RSL index points following the protocol developed by Vacchi *et al.* (2016), which has been used in a number of recent Mediterranean studies (e.g. Vacchi *et al.*, 2017, 2018; Karkani *et al.*, 2017; Fontana *et al.*, 2017; Melis *et al.*, 2017, 2018). The indicative meaning of each index point is composed of a reference water level (RWL) and the indicative range (IR). The IR corresponds to the elevation interval over which an indicator is formed and the RWL is the midpoint of this range, expressed relative to the same datum as the elevation of the sampled indicator (e.g. Horton and Shennan, 2009; Gehrels and Woodworth, 2013; Hijma *et al.*, 2015).

For the production of RSL index points from the core, we attributed an indicative range from 0 to −2 m for samples found in an open or marine-influenced lagoon and an indicative range from 0 to -1 m for an inner or semi-enclosed lagoon (Vacchi *et al.*, 2016). Although no modern analogues have been reported in the literature for the study area, the indicative ranges reported by Vacchi *et al.* (2016) have been adopted considering the geomorphological status of the coastal lagoons in the Cyclades. More precisely, in the Cycladic area, and on Paros in particular, the contemporary coastal lagoons are usually dry during the summer while, during winter, their depths do not exceed 1-2 m. We added additional vertical errors to each index point, including: a) an error of ±0.2 m for the samples altitude and b) a core stretching/shortening error of 0.15m (Hijma *et al.*, 2015).

RSL index points were further produced using samples deposited in semi-enclosed lagoon facies from Evelpidou *et al.* (2012) and from Karkani *et al.* (2018), and from samples found in a brackish environment, most likely deposited within ±0.5 m of

former MSL (Pavlopoulos *et al.*, 2011; Evelpidou *et al.*, 2012; Karkani *et al.*, 2017) (Fig. 2a). We further took into consideration the beachrock luminescence dating results from Karkani *et al.* (2017) for Paros and Naxos (Fig. 2a). Various studies in the eastern Mediterranean have shown that beachrocks are accurate sea-level indicators, as long as they are supported by cement mineralogy and morphology and, if possible, by sedimentary information (e.g. Desruelles et al., 2009; Mauz et al., 2015). The dated beachrock samples of the study area showed clear intertidal formation based on cement characteristics and therefore an indicative range between the Mean High Tide (MHT) and Mean Low Tide (MLT) (i.e. 0.14 m; HNHS, 2012) was considered (Karkani *et al.*, 2017).

To interpret the observational RSL data, we considered predictions from two Glacial Isostatic Adjustment (GIA) models. The first is ICE-6G (VM5a) of Peltier *et al.* (2015) while the second (ANU), is the latest version of the GIA model progressively developed by K. Lambeck and co-workers (see Lambeck *et al.* 2003 and further refinements). For both GIA models, we solved the Sea Level Equation using an improved version of the program SELEN (Spada and Stocchi, 2007), in which the horizontal migration of shorelines, the transition between grounded and floating ice and the rotational feedback on sea-level are taken into account. The two GIA models are characterized by different chronologies for the melting of the late-Pleistocene ice sheets but also different rheological profiles. In particular, while in ICE-6G (VM5a) the lower mantle viscosity is 3.2 10^21 Pa.s, for ANU we adopted a value 10^22 Pa.s, in the range suggested in the study of Lambeck *et al.* (2017). The relatively high lower mantle viscosity in ANU compared to ICE-6G (VM5a) generally implies a larger isostatic disequilibrium and higher rates of glacial-isostatic readjustment during the last few millennia, consistent with the results below.

175

176 **4. Results**

177 ***4.1 Lithology-faunal evidence - depositional environment***

178 Unit A: shallow marine environment

179 Unit A, from the bottom of the core (4 m) up to 2.6 m b.s.l. is dominated by medium
180 to coarse sand with shell fragments (Fig. 3, 4). The sand fraction comprises more than
181 87% of the total sediment texture. The macrofauna (Fig. 3) is dominated by
182 infralittoral sand assemblages (e.g. *Truncatella subcylindrica, Rissoa lineolate, Rissoa*
183 *monodonta, Tricolia pullus*), hard substrate assemblages (e.g. *Conus mediterraneus,*
184 *Gibbula spp., Jujubinus sp., Gibbula varia, Cythara paciniana*) and species living on
185 algae. Ostracods are almost absent with the exception of a few coastal (45.7%)
186 (*Aurila convexa, Aurila woodwardii, Cytherelloidea sordida, Hiltermannicythere cf.,*
187 *Urocythereis oblonga, Cytherois frequens, Neocytherideis fasciata, Costa edwardsii*)
188 and marine lagoonal species (54.3%) (*Loxoconcha stellifera, Xestoleberis communis,*
189 *Xestoleberis sp.*) at ~3.3 m depth (Fig. 4). This unit represents a shallow marine
190 environment. Two marine shells were dated from the middle and the top of this unit
191 (*Nassarius louisi* and *Cerithium vulgatum*, respectively; see Table 1), however, the
192 deeper sample (490±30 BP) yielded an age younger than the other shallower samples.
193 The top of the unit was dated to 964-1229 cal AD (721-986 cal BP).

194

195 Unit B: Leaky coastal lagoon

196 Unit B is found between 2.46 m and 1.18 m b.s.l., consisting of silty sand with
197 *Posidonia oceanica* fibers and shell fragments. The unit presents a finer sedimentation
198 towards the top. Gravels comprise 2.1% of the total sediment texture, sands 71.6%
199 and silts-clays 26.3%. The macrofauna is dominated by lagoonal (*Loripes lacteus,*

Abra segmentum), upper muddy sand assemblages in sheltered areas (*Acanthocardia echinata, Cerithium vulgatum*), and infralittoral sand assemblages (*Tricolia pullus, Tricolia tenius, Rissoa lineolate, Rissoa guerini, Mitra ebenus*). Microfossil assemblages are dominated by marine lagoonal (72.4%) (*Loxoconcha stellifera, Xestoleberis communis*) and coastal species (26%) (*Cytherelloidea sordida*). The middle of this unit was dated to 1652-1910 cal AD (40-298 cal BP). This unit is probably indicative of a leaky coastal lagoon, in constant connection with the sea (Kjerfve, 1994).

Unit C: Lagoon periodically connected with the sea

Unit C is found from 1.18 m b.s.l. until the top of the core and consists of coarse to medium sand, which becomes siltier towards the top. The sands fraction represents 91% of the total sediment texture up to 50 cm depth and the proportion of silts-clays increases in the last 50 cm reaching 25.4%. Macrofauna analysis indicates that assemblages are poorer in terms of abundance and mainly consist of upper muddy sand assemblages in sheltered areas (*Cerithium vulgatum*), upper-clean sand assemblages (e.g. *Conus mediterraneus, Cardita calyculata, Gibbula spp.*), hard substrate species and algae. Ostracods are dominated by marine lagoonal species (75.6%) (e.g. *Loxoconcha stellifera, Xestoleberis communis, Loxoconcha rhomboidea*); lagoonal species are represented by few individuals of *Cyprideis torosa* (3.5%), and coastal species (18.4%) (e.g. *Aurila convexa, Cytherelloidea sordida, Urocythereis oblonga, Cytherois frequens*). This unit is probably indicative of a lagoon more periodically connected with the sea ("chocked lagoon" according to the classification of Kjerfve (1994). The middle of this unit was dated to 520±30 BP.

5. Discussion

Most Cycladic islands are generally considered to be affected by a gradual subsidence, which is attributed to the crustal thinning, in an extensional tectonic regime (e.g. Mercier *et al.*, 1989; Sakellariou & Tsampouraki-Kraounaki, 2019). The absence of morphological features indicative of uplift in the coastal zone, such as marine terraces or benches, elevated beachrocks, marine notches, or raised Quaternary coastal deposits are taken to substantiate this absence of local uplift. A subsidence regime has been noted by several authors for the wider study area (e.g. Desruelles *et al.*, 2009; Lykousis, 2009; Evelpidou *et al.*, 2012; 2014; Karkani *et al.*, 2017).

The reconstructed RSL history from Paros and Naxos Islands is shown in Fig. 5. We included RSL estimates derived from archaeological data. In particular, according to Morrison (1968), a RSL rise of 5.5 m since 5500 BP may be estimated for Antiparos island, based on the Neolithic settlement of Saliagos. A RSL between -2 and -3 m around 2500–2900 BP has been estimated by Papathanassopoulos and Schilardi (1981), based on a number of archaeological findings around Paros Island (e.g. submerged moles, graves, buildings) (Fig. 5).

Overall, our new data support a RSL that rose by ~2 m in the last 2000 years, and by at least ~3.9 m since ~4500 years BP (Fig. 5). Conversely, two brackish samples from a core in Mikri Vigla (Naxos Island, Evelpidou *et al.*, 2012), indicate that RSL reached ~-2 m±0.5 at about ~4.0 ka. Similarly, two lagoonal samples from the Livadia core (Paros Island, Karkani *et al.* 2018) suggest a sea level between -1.5 and -2.5 m around 3100-3300 years BP. In both cases (Mikri Vigla and Livadia), the samples were rejected as they provided ages inconsistent with the chronostratigraphy.

In comparison with the modelled curves, which account for the effect of GIA, for Paros Island (Fig. 5), our RSL points have a lower position. To evaluate the tectonic component, we subtracted the elevation of the produced index points, from that of the corresponding points inferred from the GIA models at the same age (e.g. Chelli *et al.*, 2017). Average rates of tectonic subsidence were calculated for three different time frames (present to ~5500 cal BP, present day to 2500 cal BP, 2500 cal BP to 5500 cal BP), based on the mismatch between models and observations for Paros and the wider study area, considering the difference in elevation between sea level estimates from our data and from each of the models employed.

Since ~5500 cal BP, comparable tectonic subsidence rates (~ 1.0±0.4 mm/yr) are found when the RSL data are corrected for the predictions of the two GIA models. The average rate of tectonic subsidence appears lower for the timespan 2500-5000 cal BP, being close to 0.7±0.2 mm/yr, and higher (~1.2±0.4 mm/yr) since 2500 cal BP. It appears evident from our findings that subsidence rates in the central Cyclades (Paros and Naxos) have not been constant since ~5500 cal BP. This suggests that, since ~2500 cal BP, the study area has been affected by seismic events that produced vertical displacements and/or during this time span the subsidence rate increased. Evidence of seismic events, since about 3300 BP, have been reported in the study area by Evelpidou *et al.* (2014) through the analysis of submerged tidal notches, suggesting that at least part of the observed subsidence is related to vertical seismic displacements. Evelpidou *et al.* (2014) identified former shorelines at depths between 280 ± 20 and 30 ± 5 cm below modern sea level. In a recent study Vamvakaris *et al.* (2016), calculated the mean return period values for shallow earthquakes with M>6.0 in the Aegean region and suggested very long return periods (> 200 years) for the broader Cyclades plateau, amongst other areas. The same authors also found that the

most probable maximum magnitudes for a return period of 50 yr is expected to be less than M=5.0, for low seismicity areas, such as the Cyclades islands plateau. In the Cyclades, one of the largest earthquakes in the last century occurred in July 1956, southwest of Amorgos Island, with a magnitude of 7.4, which was followed (a few minutes later) by a second of Ms 7.2 (e.g. Stiros et al., 1994; Okal *et al.*, 2009; Brüstle *et al.*, 2014).

For decades the Cycladic plateau has been considered as a tectonically inactive area (Sakellariou and Tsampouraki-Kraounaki, 2019). Our findings suggest that tectonic subsidence has contributed to the late Holocene evolution of the central Cyclades and it is most likely owed to a combination of seismic events and gradual long-term subsidence, due to the dominance of an extensional structural pattern. Furthermore, subsidence rates are higher than previously calculated for the study area (e.g. Pavlopoulos *et al.*, 2011).

6. Conclusions

Our study focused on the reconstruction of RSL changes in the central Cyclades through the analysis of new and published sea-level data. We reevaluated the tectonic regime of the central Cyclades through the comparison of our data with new modelled RSL curves for Paros Island. Our findings suggest average tectonic subsidence rates close to 1 mm/yr since 5500 cal BP, which do not appear constant during the late Holocene; these values have increased since 2500 cal BP. The subsidence trend in the central Cyclades is most likely a combination of seismic events and gradual long-term subsidence, due to the dominance of an extensional structural pattern.

Acknowledgements

The authors would like to thank Alexandros Petropoulos, Giannis Saitis, Theophilos Valsamidis, Matina Seferli and Electra Kotopoulou for their help during fieldwork in Paros.

This work was co-funded by the General Secretariat for Research and Technology (GSRT) and the European Regional Development Fund, in the framework of the Bilateral project Greece – France entitled: 'Sea level changes in Cyclades'.

This work has been partially carried out thanks to the support of the Labex OT-Med (ANR-11-LABX-0061) and of the A*MIDEX project (n° ANR-11-IDEX-0001-02), funded by the « Investissements d'Avenir» French Government program, managed by the French National Research Agency (ANR).

GS is funded by a FFABR (Finanziamento delle Attività Base di Ricerca) grant of the MIUR (Ministero dell'Istruzione, dell'Università e della Ricerca) and by a DiSPeA research grant.

Figure captions

Fig. 1. Location of the study area and seismicity since 550 B.C. (seismicity data retrieved from http://geophysics.geo.auth.gr/ss/station_index_en.html). The red square denotes the location of Paros Island. The bathymetry was provided by EMODnet Bathymetry 2015.

Fig. 2: a) Location of the drilling site on Paros Island and sea-level data used in this study from Evelpidou *et al.* (2012) and Karkani *et al.* (2017; 2018), b) Aerial view of Pounta coring site.

Fig. 3. Core POU2 stratigraphy and macrofauna.

Fig. 4. Core POU2 stratigraphy and ostracods.

Fig. 5: Late Holocene RSL data from this study, compared with beachrock data from Karkani *et al.* (2017) and sediment corings from Paros (Karkani et al., 2018) and Naxos (Evelpidou *et al.*, 2012). The circled samples are in disagreement with the rest of RSL index points. The RSL curves for Paros Island were obtained by numerically solving the Sea-Level Equation. The GIA models ICE-6G (solid) and ANU (dashed) have been employed.

Table captions

Table 1. Radiocarbon ages for dated samples from the Paros core. The data were calibrated using the online software Calib 7.10 (Stuiver *et al.*, 2016) with the Marine13 curve (Reimer *et al.*, 2013). Shell samples were corrected for the local marine reservoir effect according to Reimer & McCormac (2002), using a mean ΔR value of 154 ± 52 for the Aegean Sea.

References

Bargnesi, E.A., Stockli, D.F., Mancktelow, N., Soukis, K., 2013. Miocene core complex development and coeval supradetachment basin evolution of Paros, Greece, insights from (U–Th)/He thermochronometry. Tectonophysics 595–596, 165–182. doi:10.1016/j.tecto.2012.07.015

Bradley, S. L., Milne, G. A., Horton, B. P., Zong, Y., 2016. Modelling sea level data from China and Malay-Thailand to estimate Holocene ice-volume equivalent sea level change. Quaternary Science Reviews 137, 54–68. https://doi.org/10.1016/J.QUASCIREV.2016.02.002

Brüstle, A., Friederich, W., Meier, T., Gross, C., 2014. Focal mechanism and depth of the 1956 Amorgos twin earthquakes from waveform matching of analogue

seismograms. Solid Earth 5, 1027-1044, https://doi.org/10.5194/se-5-1027-2014, 2014.

Chelli, A., Pappalardo, M., Bini, M., Brückner, H., Neri, G., Neri, M., Spada, G., 2017. Assessing tectonic subsidence from estimates of Holocene relative sea-level change: An example from the NW Mediterranean (Magra Plain, Italy). The Holocene 27(12), 1988–1999. https://doi.org/10.1177/0959683617715688

Church, J.A., White, N.J., Aarup, T., Wilson, W.S., Woodworth, P.L., Domingues, C.M., Hunter, J.R., Lambeck, K., 2008. Understanding global sea levels: past, present and future. Sustain. Sci. 3, 9-22.

d'Angelo, G., Gargiullo, S., 1978. Guida alle conchiglie Mediterranee. Fabbri Editori, Milano.

Desruelles, S., Fouache, É., Ciner, A., Dalongeville, R., Pavlopoulos, K., Kosun, E., Coquinot, Y., Potdevin, J.-L., 2009. Beachrocks and sea level changes since Middle Holocene: Comparison between the insular group of Mykonos–Delos–Rhenia (Cyclades, Greece) and the southern coast of Turkey. Global and Planetary Change 66, 19–33. doi:10.1016/j.gloplacha.2008.07.009

Doneddu, M., Trainito, E., 2005. Conchiglie del Mediterraneo. Il Castello, Trezzano sul Naviglio.

Engelhart, S.E., Horton, B.P., 2012. Holocene sea level database for the Atlantic coast of the United States. Quaternary Science Reviews 54, 12-25.

Engelhart, S.E., Horton, B.P., Douglas, B.C., Peltier, W.R., Horton, B.P., Tornqvist, T.E., 2009. Spatial variability of late Holocene and 20th century sea-level rise along the Atlantic coast of the United States. Geology 37, 1115-1118.

372 Evelpidou, N., Pavlopoulos, K., Vassilopoulos, A., Triantafyllou, M., Vouvalidis, K.,
373 Syrides, G., 2012. Holocene palaeogeographical reconstruction of the western part
374 of Naxos island (Greece). Quaternary International 266, 81-93.
375 Evelpidou, N., Melini, D., Pirazzoli, P., Vassilopoulos, A., 2014. Evidence of
376 repeated Late Holocene subsidence in the SE Cyclades (Greece) deduced from
377 submerged notches. International Journal of Earth Sciences 103 (1), 381-395. doi:
378 10.1007/s00531-013-0942-0.
379 Fontana, A., Vinci, G., Tasca, G., Mozzi, P., Vacchi, M., Bivi, G., Salvador, S.,
380 Rossato, S., Antonioli, F., Asioli, A., Bresolin, M., Di Mario, F., Hajdas, I., 2017.
381 Lagoonal settlements and relative sea level during Bronze Age in Northern
382 Adriatic: Geoarchaeological evidence and paleogeographic constraints. Quaternary
383 International 439, 17–36. https://doi.org/10.1016/j.quaint.2016.12.038
384 Gehrels, W.R., Woodworth, P.L., 2013. When did modern rates of sea-level rise start?
385 Global and Planetary Change 100, 263-277. DOI: 10.1016/j.gloplacha.2012.10.020
386 Hellenic Navy Hydrographic Service (HNHS), 2012. Statistical data for sea level of
387 the Greek ports. HNHS, Athens (in Greek).
388 Hijma, M.P., Engelhart, S.E., Törnqvist, T.E., Horton, B.P., Hu, P., Hill, D.F., 2015.
389 A protocol for a geological sea-level database. In: Shennan, I., Long, A., Horton,
390 B.P. (Eds.), Handbook of Sea-Level Research. Willey, pp. 536–553.
391 doi:10.1002/9781118452547.ch34
392 Horton, B.P., Shennan, I., 2009. Compaction of Holocene strata and the implications
393 for relative sea level change on the east coast of England. Geology 37, 1083-1086.
394 Kapsimalis, V., Pavlopoulos, K., Panagiotopoulos, I., Drakopoulou, P., Vandarakis,
395 D., Sakelariou, D., Anagnostou, C., 2009. Geoarchaeological Challenges in the

Cyclades Continental Shelf (Aegean Sea). Zeitschrift für Geomorphologie 53 (Suppl. 1), 169-190.

Karkani, A., Evelpidou, N., Vacchi, M., Morhange, C., Tsukamoto, S., Frechen, M., Maroukian, H., 2017. Tracking shoreline evolution in central Cyclades (Greece) using beachrocks. Marine Geology 388, 25–37. https://doi.org/10.1016/j.margeo.2017.04.009

Karkani, A., Evelpidou, N., Giaime, M., Marriner, N., Maroukian, H., Morhange, C., 2018. Late Holocene palaeogeographical evolution of Paroikia Bay (Paros Island, Greece). Comptes Rendus Geoscience 350 (5), 202-211. https://doi.org/10.1016/j.crte.2018.04.004

Kjerfve, B., 1994. Coastal Lagoons. In: Kjerfve, B. (Ed.), Coastal Lagoon Processes. Elsevier, pp. 1-8. https://doi.org/doi:10.1201/EBK1420088304-c1

Lachenal, A.M., 1989. Écologie des ostracodes du domaine méditerranéen: application au Golfe de Gabès (Tunisie orientale). Les variations du niveau marin depuis 30 000 ans. Documents des laboratoires de géologie de Lyon 108, 1–239.

Lambeck, K., Purcell, A., Johnston, P., Nakada, M., Yokoyama, Y., 2003. Water-load definition in the glacio-hydro-isostatic sea-level equation. Quaternary Science Reviews 22(2), 309-318.

Lambeck, K., Antonioli, F., Purcell, A., Silenzi, S., 2004. Sea-level change along the Italian coast for the past 10,000 yr. Quaternary Science Reviews 23, 1567-1598.

Lykousis, V., 2009. Sea-level changes and shelf break prograding sequences during the last 400ka in the Aegean margins: Subsidence rates and palaeogeographic implications. Continental Shelf Research 29, 2037–2044. doi:10.1016/j.csr.2008.11.005

Mauz, B., Vacchi, M., Green, A., Hoffmann, G., Cooper, A., 2015. Beachrock: A tool for reconstructing relative sea level in the far-field. Marine Geology 362, 1–16. https://doi.org/10.1016/j.margeo.2015.01.009

Melis, R.T., Depalmas, A., Di Rita, F., Montis, F., Vacchi, M., 2017. Mid to late Holocene environmental changes along the coast of western Sardinia (Mediterranean Sea). Global and Planetary Change 155, 29–41. https://doi.org/10.1016/J.GLOPLACHA.2017.06.001

Melis, R. T., Di Rita, F., French, C., Marriner, N., Montis, F., Serreli, G., Sulas, F., Vacchi, M., 2018. 8000 years of coastal changes on a western Mediterranean island: A multiproxy approach from the Posada plain of Sardinia. Marine Geology 403, 93–108. https://doi.org/10.1016/j.margeo.2018.05.004

Mercier, J.-L., Sorel, D., Vergely, P., Simeakis, K., 1989. Extensional tectonic regimes in the Aegean basins during the Cenozoic. Basin Research 2, 49–71

Milne, G.A., Long, A.J., Bassett, S.E., 2005. Modelling Holocene relative sea-level observations from the Caribbean and South America. Quaternary Science Reviews 24, 1183-1202.

Morrison, I.A., 1968. Appendix I. Relative sea-level change in the Saliagos area since Neolithic times. In: Evans, J.D., Renfrew, C. (Eds.), Excavations at Saliagos Near Antiparos. Thames and Hudson, London, pp. 92-98.

Nachite, D., Rodríguez-Lázaro, J., Martín-Rubio, M., Pascual, A., Bekkali, R., 2010. Distribution and ecology of recent ostracods from the Tahadart estuary (NW Morocco). Revue de Micropaleontologie 53, 3–15.

Okal, E., Synolakis, C., Uslu, B., Kalligeris, N., Voukouvalas, E., 2009. The 1956 earthquake and tsunami in Amorgos, Greece. Geophysical Journal International 178, 1533–1554.

445 Papanikolaou, D., 1996. Geological map of Paros, scale 1:50000. IGME, Athens (in
446 Greek).
447 Papathanassopoulos, G., Schilardi, D., 1981. An underwater survey of Paros, Greece:
448 1979. Preliminary report. The International Journal of Nautical Archaeology and
449 Underwater Exploration 10 (2), 133-144.
450 Papazachos, B.C., 1990. Seismicity of the Aegean and surrounding area.
451 Tectonophysics 178, 287–308. doi:10.1016/0040-1951(90)90155-2
452 Pavlopoulos, K., Kapsimalis, V., Theodorakopoulou, K., Panagiotopoulos, I.P., 2011.
453 Vertical displacement trends in the Aegean coastal zone (NE Mediterranean)
454 during the Holocene assessed by geo-archaeological data. The Holocene 22 (6),
455 717-728.
456 Peltier, W.R., 2002. On eustatic sea level history: Last Glacial Maximum to
457 Holocene. Quat. Sci. Rev. 21, 377-396.
458 Peltier, W.R., 2004. Global glacial isostasy and the surface of the ice-age earth: the
459 ice-5G (VM2) model and grace. Annual Review of Earth and Planetary Sciences
460 32, 111-149.
461 Peltier, W.R., Argus, D.F., Drummond, R., 2015. Space geodesy constrains ice age
462 terminal deglaciation: the global ICE-6G-C (VM5a) model. Journal of Geophysical
463 Research B: Solid Earth 120(1), 450–487. doi: 10.1002/2014JB011176.
464 Pérès, J.-M., 1982. Major benthic assemblages. In: Kinne, O. (Ed.), Marine Ecology.
465 Wiley, Chichester, pp. 373–522.
466 Pérès, J.-M., Picard, J., 1964. Nouveau manuel de bionomie benthique de la mer
467 Méditerranée. Periplus, Marseille, 137 p.
468 Pirazzoli, P.A., 2005. A review of possible eustatic, isostatic and tectonic
469 contributions in eight late-Holocene relative sea-level histories from the

Mediterranean area. Quaternary Science Reviews 24 (18-19), 1989-2001. https://doi.org/10.1016/j.quascirev.2004.06.026

Reimer, P.J., McCormac, F.G., 2002. Marine radiocarbon reservoir corrections for the Mediterranean and Aegean Seas. Radiocarbon 44, 159-166.

Reimer, P.J., Bard, E., Bayliss, A., Beck, J.W., Blackwell, P.G., Bronk Ramsey, C., Buck, C.E., Cheng, H., Edwards, R.L., Friedrich, M., Grootes, P.M., Guilderson, T.P., Haflidason, H., Hajdas, I., Hatté, C., Heaton, T.J., Hoffmann, D.L., Hogg, A.G., Hughen, K.A., Kaiser, K.F., Kromer, B., Manning, S.W., Niu, M., Reimer, R.W., Richards, D.A., Scott, E.M., Southon, J.R., Staff, R.A., Turney, C.S.M., van der Plicht, J., 2013. IntCal13 and Marine13 radiocarbon age calibration curves 0–50,000 years cal BP. Radiocarbon 55(4), 1869–1887.

Rovere, A., Stocchi, P., Vacchi, M., 2016. Eustatic and Relative Sea Level Changes. Current Climate Change Reports 2, 221–231. doi:10.1007/s40641-016-0045-7

Rovere, A., Furlani, S., Benjamin, J., Fontana, A., Antonioli, F., 2012. MEDFLOOD project: MEDiterranean sea-level change and projection for future FLOODing. Alpine and Mediterranean Quaternary 25, 3–5.

Sakellariou, D., Galanidou, N., 2016. Pleistocene submerged landscapes and Palaeolithic archaeology in the tectonically active Aegean region. Geological Society of London, Special Publication 411, 145–178. doi:10.1144/SP411.9

Sakellariou, D., Tsampouraki-Kraounaki, K., 2019. Plio-Quaternary Extension and Strike-Slip Tectonics in the Aegean. In: Duarte, J. (Ed.), Transform Plate Boundaries and Fracture Zones. Elsevier, pp. 339–374. https://doi.org/10.1016/B978-0-12-812064-4.00014-1

493 Salel, T., Bruneton, H., Lefèvre, D., 2016. Ostracods and environmental variability in
494 lagoons and deltas along the north-western Mediterranean coast (Gulf of Lions,
495 France and Ebro delta, Spain). Revue de Micropaléontologie 59 (4) 425-444.
496 Sivan, D., Wdowinski, S., Lambeck, K., Galili, E., Raban, A., 2001. Holocene sea-
497 level changes along the Mediterranean coast of Israel, based on archaeological
498 observations and numerical model. Palaeogeography, Palaeoclimatology,
499 Palaeoecology 167(1–2), 101–117. https://doi.org/10.1016/S0031-0182(00)00234-
500 0
501 Sivan, D., Lambeck, K., Toueg, R., Raban, A., Porath, Y., Shirman, B., 2004. Ancient
502 coastal wells of Caesarea Maritima, Israel, an indicator for relative sea level
503 changes during the last 2000 years. Earth and Planetary Science Letters 222, 315-
504 330. https://doi.org/10.1016/j.epsl.2004.02.007
505 Spada G, Stocchi P (2007) SELEN: a Fortran 90 program for solving the “Sea level
506 equation”. Computers & Geosciences 33(4), 538-562.
507 Stiros, S.C., Marangou, L., Arnold, M., 1994. Quaternary uplift and tilting of
508 Amorgos Island (southern Aegean) and the 1956 earthquake. Earth and Planetary
509 Science Letters 128(3-4), 65-76.
510 Stiros, S.C., Laborel, J., Laborel-Deguen, F., Morhange, C., 2011. Quaternary and
511 Holocene coastal uplift in Ikaria Island, Aegean Sea. Geodinamica Acta 24 (3-4),
512 123-131. doi:10.3166/ga.24.123-13
513 Stuiver, M., Reimer, P.J., and Reimer, R.W., 2016.CALIB 7.1 [WWW program] at
514 http://calib.org, accessed 2016-12-4.
515 Tirel, C., Gueydan, F., Tiberi, C., Brun, J.P., 2004. Aegean crustal thickness inferred
516 from gravity inversion. Geodynamical implications. Earth and Planetary Science
517 Letters 228, 267–280. doi:10.1016/j.epsl.2004.10.023

Vacchi, M., Marriner, N., Morhange, C., Spada, G., Fontana, A., Rovere, A., 2016. Multiproxy assessment of Holocene relative sea-level changes in the western Mediterranean: Sea-level variability and improvements in the definition of the isostatic signal. Earth-Science Reviews 155, 172–197. https://doi.org/10.1016/j.earscirev.2016.02.002

Vacchi, M., Ghilardi, M., Spada, G., Currás, A., Robresco, S., 2017. New insights into the sea-level evolution in Corsica (NW Mediterranean) since the late Neolithic. Journal of Archaeological Science: Reports 12, 782–793. https://doi.org/10.1016/j.jasrep.2016.07.006

Vacchi, M., Ghilardi, M., Melis, R. T., Spada, G., Giaime, M., Marriner, N., Lorscheid, T., Morhange, C., Burjachs, F., Rovere, A., 2018. New relative sea-level insights into the isostatic history of the Western Mediterranean. Quaternary Science Reviews 201, 396–408. https://doi.org/10.1016/J.QUASCIREV.2018.10.025

Vamvakaris, D.A., Papazachos, C.B., Papaioannou, C.A., Scordilis, E.M., Karakaisis, G.F., 2016. A detailed seismic zonation model for shallow earthquakes in the broader Aegean area. Natural Hazards and Earth System Sciences 16, 55–84. doi:10.5194/nhess-16-55-2016

Van De Plassche, O., Wright, A. J., Horton, B. P., Engelhart, S. E., Kemp, A. C., Mallinson, D., Kopp, R. E., 2014. Estimating tectonic uplift of the Cape Fear Arch (south-eastern United States) using reconstructions of Holocene relative sea level. Journal of Quaternary Science 29(8), 749–759. https://doi.org/10.1002/jqs.2746

Woodroffe, S. A., Long, A. J., Milne, G. A., Bryant, C. L., Thomas, A. L., 2015. New constraints on late Holocene eustatic sea-level changes from Mahé, Seychelles.

542 Quaternary Science Reviews, 115, 1–16.

543 https://doi.org/10.1016/J.QUASCIREV.2015.02.011

Table 1. Radiocarbon ages for dated samples from the Paros core. The data were calibrated using the online software Calib 7.10 (Stuiver et al., 2016) with the Marine13 curve (Reimer et al., 2013). Shell samples were corrected for the local marine reservoir effect according to Reimer & McCormac (2002), using a mean ΔR value of 154 ± 52 for the Aegean Sea.

Sample code	Lab code	Depth below sea level (m)	Material	$\delta^{13}C$	^{14}C BP	Age cal. BP	Cal. BC/AD (2σ)
POU2-1	Poz-81147	85	Conus mediterraneus	2.8	520±30	-	-
POU2-2	Poz-81148	186-196	Loripes lacteus	0.3	715±30	40-298	1652-1910 AD
POU2-3	Poz-81354	260-270	Cerithium vulgatum	-3.9	1475±30	721-986	964-1229 AD
POU2-4	Poz-81140	337-346	Nassarius louisi	4.9	490±30	-	-

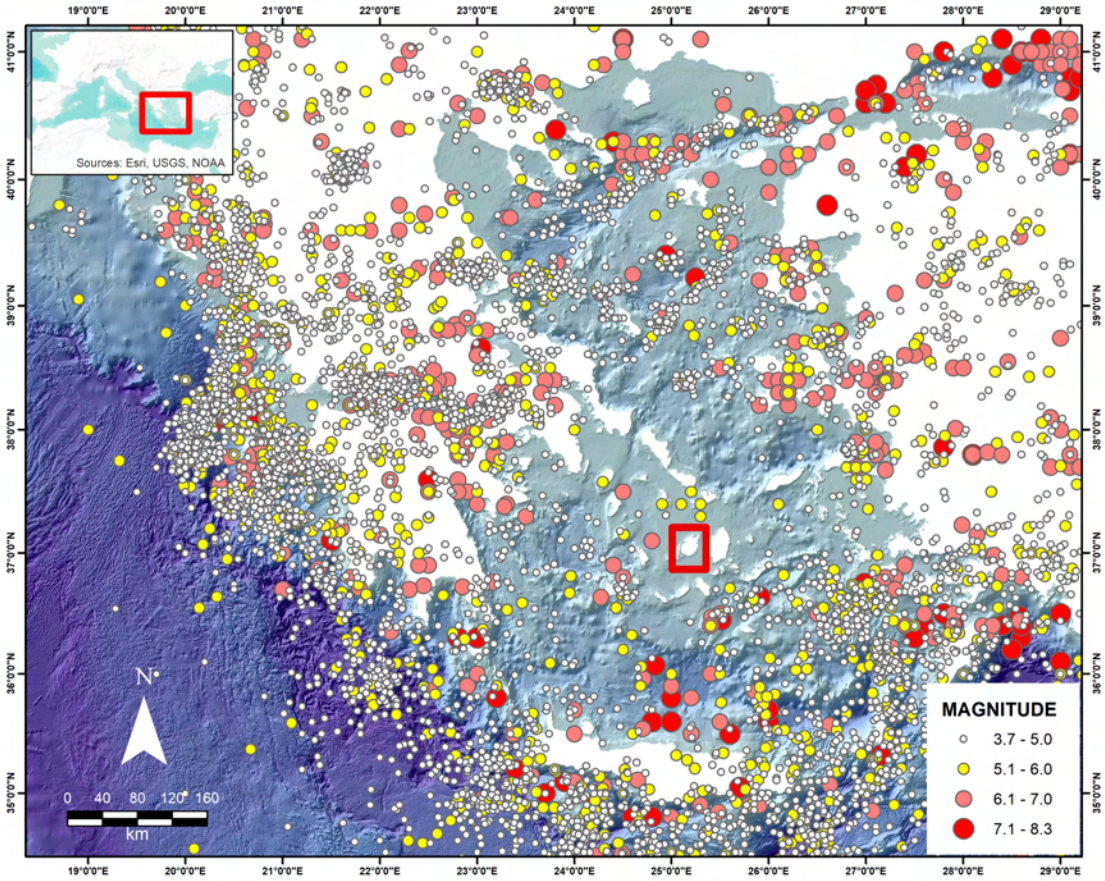

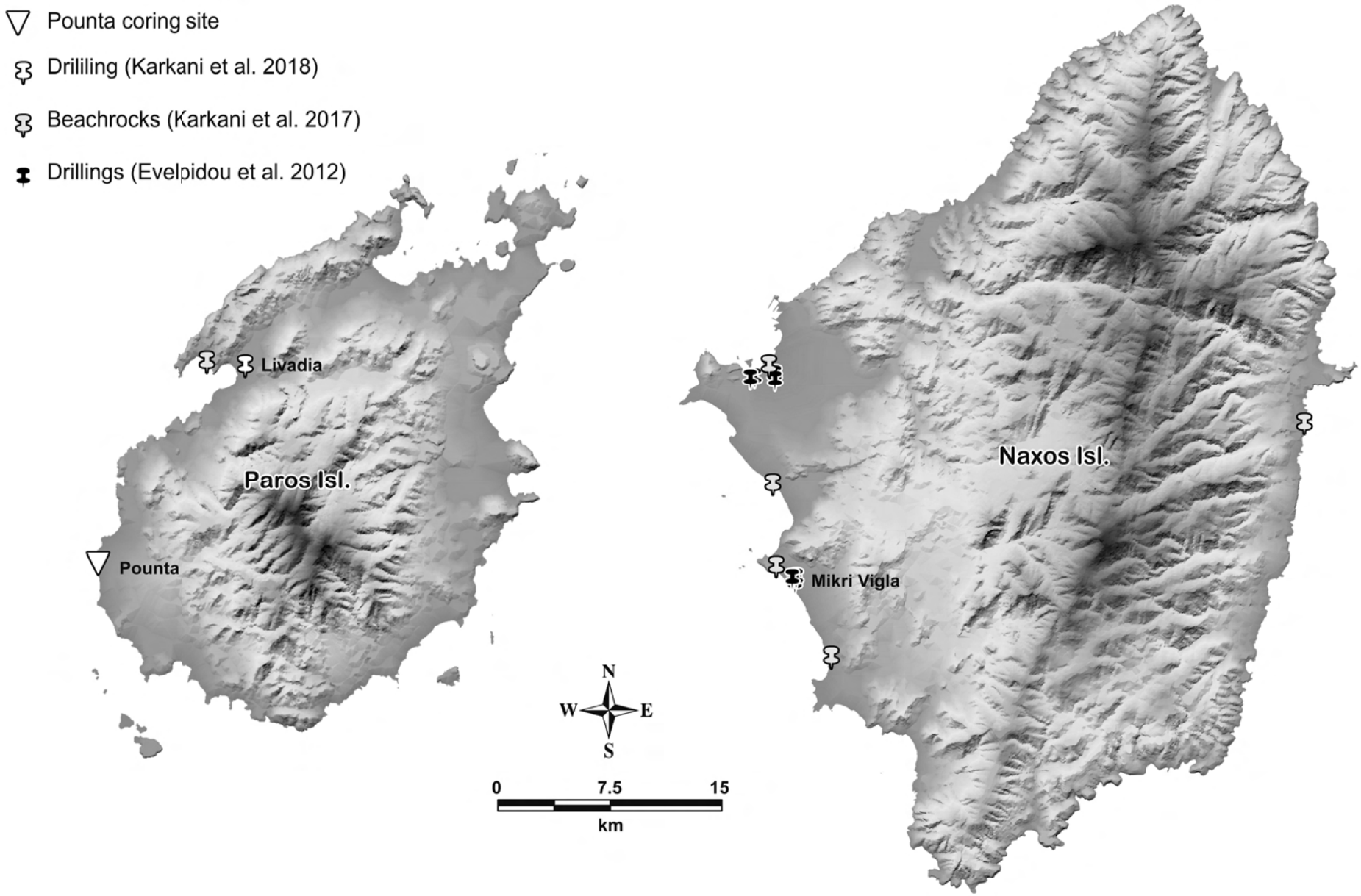
Pounta coring site
Drililing (Karkani et al. 2018)
Beachrocks (Karkani et al. 2017)
Drillings (Evelpidou et al. 2012)
Livadia
Paros Isl.
Pounta
Naxos Isl.
Mikri Vigla
N
W
E
S
0
7.5
15
km

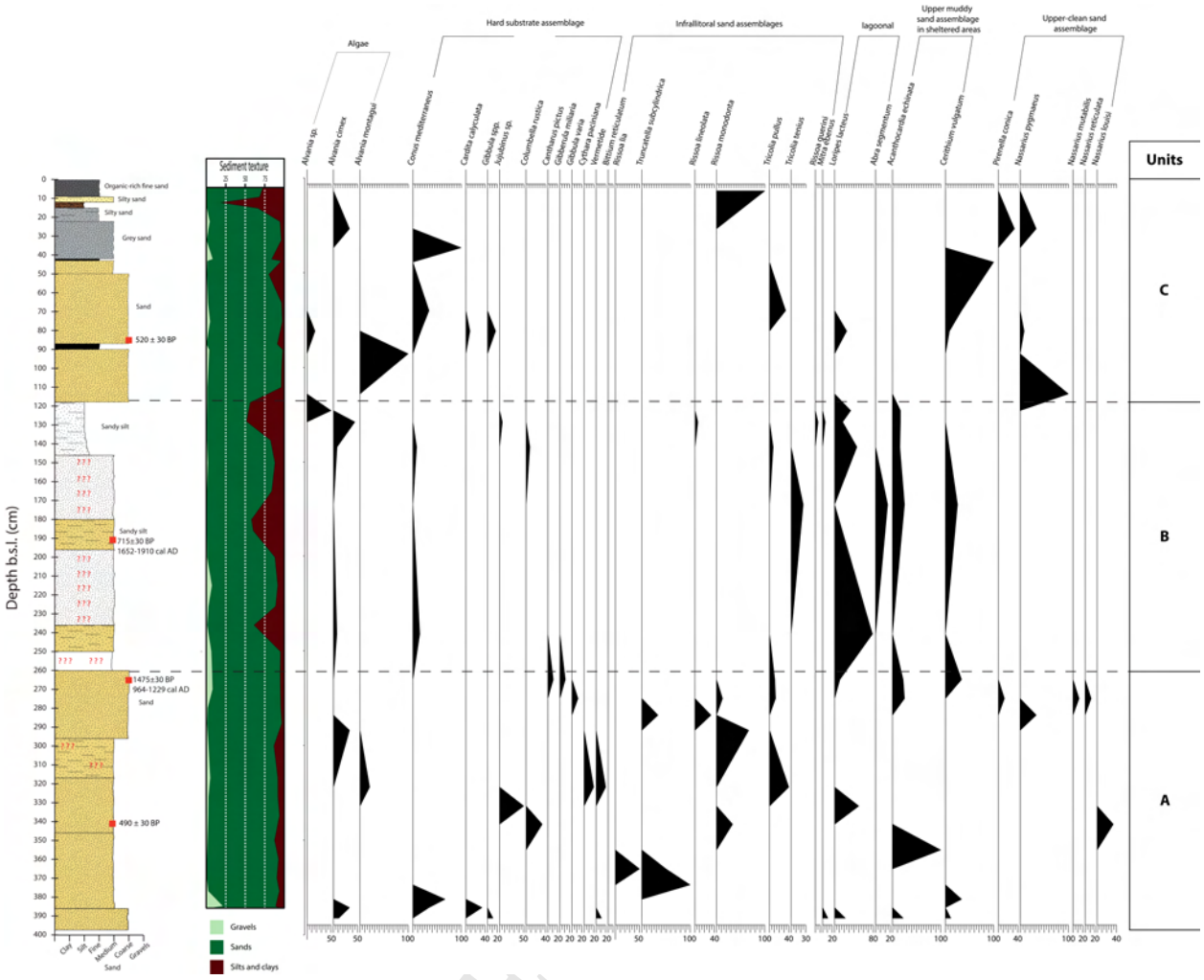
Depth b.s.l. (cm)
Organic-rich fine sand
Silty sand
Silty sand
Grey sand
Sand
520 ± 30 BP
Sandy silt
Sandy silt
715±30 BP
1652-1910 cal AD
1475±30 BP
964-1229 cal AD
Sand
490 ± 30 BP
Clay
Silt
Fine
Medium
Coarse
Gravels
Sand
Sediment texture
Gravels
Sands
Silts and clays
Algae
Hard substrate assemblage
Infrallitoral sand assemblages
lagoonal
Upper muddy sand assemblage in sheltered areas
Upper-clean sand assemblage
Alsania sp.
Alsania corvex
Alsania montagui
Conus mediterraneus
Caratia calyculata
Gibbula spp.
Jujubinus sp.
Columbella rustica
Cantharus picta
Globularia mallea
Globularia varia
Cythara pacinina
Vermetidae
Bittium reticulatum
Rissoa lia
Truncatella subcylindrica
Rissoa lineolata
Rissoa monodonta
Tricolia pullus
Tricolia tenuis
Rissoa guerini
Rissoa venusta
Loripes lacteus
Abra segmentum
Acanthocardia echinata
Cerithium vulgatum
Pirenella conica
Nassarius pygmaeus
Nassarius mutabilis
Nassarius reticulata
Nassarius fossil
Units
C
B
A

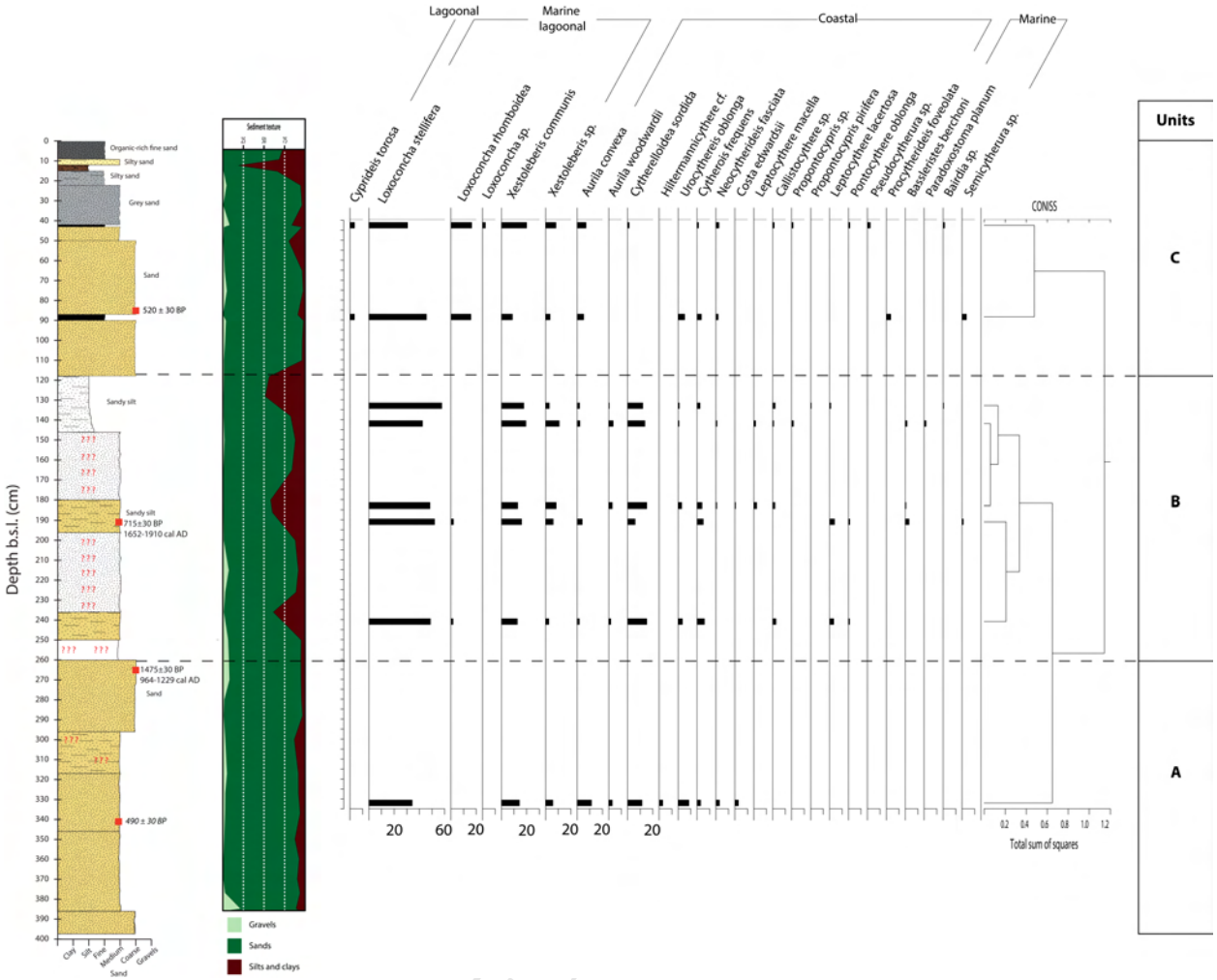
Lagoonal
Marine lagoonal
Coastal
Marine
Cyprideis torosa
Loxoconcha stellifera
Loxoconcha rhomboidea
Loxoconcha sp.
Xestoleberis communis
Xestoleberis sp.
Aurila convexa
Aurila woodwardii
Cytherelloidea sordida
Hiltermannicythere cf.
Urocytherois oblonga
Cytherois frequens
Neocytheridea fasciata
Costa edwardsii
Leptocythere macella
Callistocythere sp.
Propontocypris sp.
Propontocypris pirifera
Leptocythere lacertosa
Pontocythere oblonga
Pseudocytherura sp.
Procytheridea foveolata
Basileistes berchoni
Paradoxostoma planum
Baldia sp.
Semicytherura sp.
CONISS
Units
C
B
A
Depth b.s.l. (cm)
Organic-rich fine sand
Silty sand
Silty sand
Grey sand
Sand
520 ± 30 BP
Sandy silt
Sandy silt
715±30 BP
1652-1910 cal AD
1475±30 BP
964-1229 cal AD
Sand
490 ± 30 BP
Clay
Silt
Fine
Medium
Coarse
Gravels
Sand
Sediment texture
Gravels
Sands
Silts and clays
20
60
20
20
20
20
20
0.2
0.4
0.6
0.8
1.0
1.2
Total sum of squares

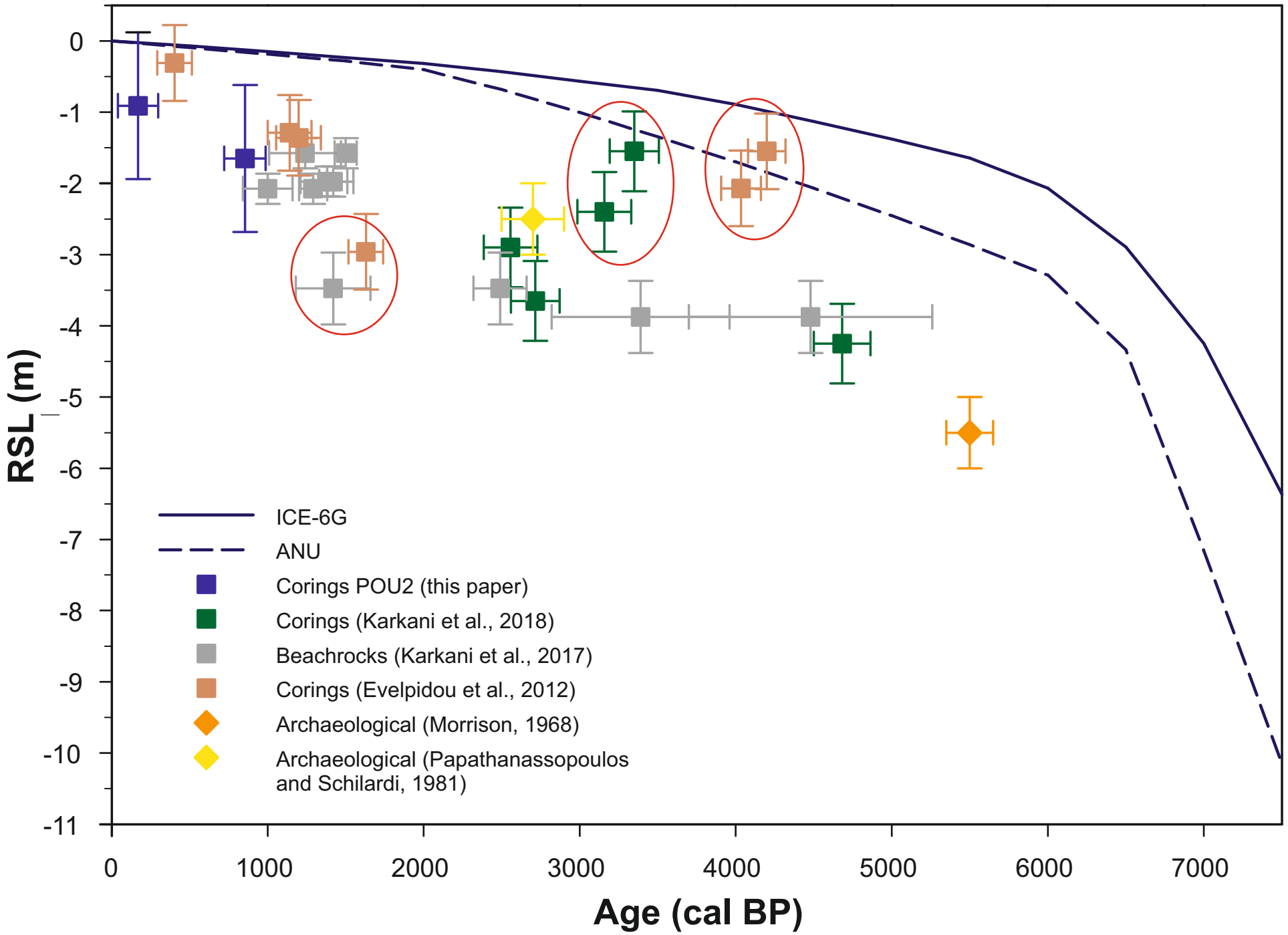
RSL (m)
0
-1
-2
-3
-4
-5
-6
-7
-8
-9
-10
-11
0
1000
2000
3000
4000
5000
6000
7000
Age (cal BP)
ICE-6G
ANU
Corings POU2 (this paper)
Corings (Karkani et al., 2018)
Beachrocks (Karkani et al., 2017)
Corings (Evelpidou et al., 2012)
Archaeological (Morrison, 1968)
Archaeological (Papathanassopoulos and Schilardi, 1981)